ACS APPLIED MATERIALS & INTERFACES

Research Article

www.acsami.org

Ultracompressible, High-Rate Supercapacitors from Graphene-Coated Carbon Nanotube Aerogels

Evan Wilson and Mohammad F. Islam*

Department of Materials Science & Engineering, Carnegie Mellon University, 5000 Forbes Avenue, Pittsburgh, Pennsylvania 15213, United States

Supporting Information

ABSTRACT: Emerging applications for electrochemical energy storage require devices that not only possess high power and energy, but also are capable of withstanding mechanical deformation without degradation of performance. To this end, we have constructed electric double layer capacitors (EDLCs), also referred to as supercapacitors, using thick, ultracompressible graphene-coated carbon nanotube aerogels as electrodes. These electrodes showed a high capacitance in both aqueous and room-temperature ionic liquid (RTIL) electrolytes, achieving between 60 and100 F/g, respectively, with the performance stable over hundreds of charge/discharge cycles and at high rates exceeding 1 V/s. This performance was retained fully under 90% compression of the systems, allowing us to construct cells with high volumetric capacitances of ∼5−18 F/cm^3 in aqueous and RTIL electrolytes, respectively, which are 50−100 times higher than comparable compressible EDLCs (∼0.1 F/cm^3). Further, the volumetric capacitances approach values reported for compressible pseudocapacitors (∼15−30 F/cm^3) but without the degraded lifetime and reversibility that typically plague compressible pseudocapacitors. The electrodes demonstrated largely strain-invariant ion transport with no change in capacitance and high-rate performance even at 90% compressive strain. This material serves as an excellent platform for exploring the possibility for use of extremely compressible EDLCs with negligible degradation in capacitance in applications such as electric vehicles and wearable electronics.

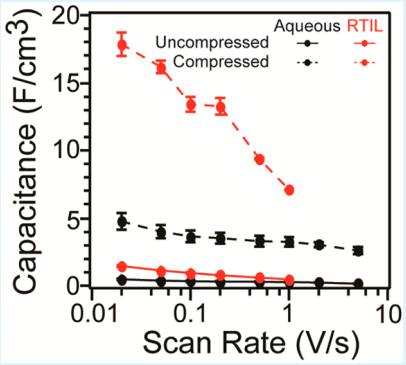

KEYWORDS: *supercapacitors, ultracompressible, carbon nanotubes, graphene, aerogels*

INTRODUCTION

To keep pace with the growing prevalence of portable electronic devices, electric vehicles, and many other emerging applications, there has been significant research effort toward better understanding and engineering of lightweight electrochemical energy storage devices that are mechanically robust and retain performance under diverse loading conditions such as bending, stretching, or compression. Within this research, electric double layer capacitors (EDLCs), also called supercapacitors, have received tremendous attention. EDLCs work by storing charge in the form of solvated ions on the surface of a porous conductive electrode.[1,2] Because EDLCs involve only ionic adsorption/desorption and do not rely on chemical reactions, electrode kinetics are rapid and reversible, resulting in power significantly higher than other electrochemical energy sources (e.g., lithium-ion batteries and pseudocapacitors).[3,4] However, the lack of chemical reactions means the energy density of an EDLC is often much lower than that of a Lithium-ion battery or a pseudocapacitor.[3,5]

Because the energy stored on an electrode scales with the square of the voltage, careful engineering and selection of the electrolyte has led to increased energy from an expanded operating voltage. For example, EDLCs that utilize a room temperature ionic liquid (RTIL) as electrolyte can achieve voltage windows at or exceeding 3 V, as opposed to ∼1.2 V for aqueous electrolyte based EDLCs.[6,7] Electrolyte engineering is a complex problem, however, and advances have been limited. In contrast, significant research effort has focused on increasing the stored energy through use of high surface area electrodes such as activated carbons, which can have specific surface areas approaching or in excess of 3000 m^2/g.[1,4,8,9] However, most of this surface area comes from pores that are too small to be accessible to ions, often giving a capacitance significantly lower than the theoretical value of ∼300 F/g.[8−10] As a result, researchers have shaped nanoscale carbons such as graphene, carbon nanotubes, and many others into electrodes that maintain high specific surface area while having pores that allow for improved ionic infiltration.[1,2,4,11−19] Because all of the surface area is available, EDLCs utilizing these electrodes display improved stability, charge/discharge rate, and reversible gravimetric capacitance often well beyond 100 F/g and in some cases nearly 300 F/g in aqueous electrolytes and nearly identical performance for most systems in RTIL electrolytes.[4,20−22] Another important consideration to improve EDLC performance is to make thicker electrodes, which in turn requires fewer current collectors and other expensive and

Received: February 11, 2015
Accepted: February 20, 2015
Published: February 20, 2015

DOI: 10.1021/acsami.5b01384
ACS Appl. Mater. Interfaces 2015, 7, 5612−5618

Table 1. Comparison of Compressible Electrochemical Capacitor Electrode Materials

density (mg/mL)	specific surface area (m^2/g)	pseudocapacitive	uncompressed capacitance	maximum rate (mV/s)	maximum compression (%)	compressed capacitance	ref
7−14	700	no	60−100 F/g 1 F/cm^3	5000	90	60−100 F/g 5−18 F/cm^3	this work
10−20	90−100	no	1.12 F/g 0.075 F/cm^3	1000	50	1.08 F/g 1.25 F/cm^3	ref 31
5−8	463	yes	360 F/g 14 F/cm^3	30	50	360 F/g 28 F/cm^3	ref 34
~30[a]	108	yes	320 F/g 9 F/cm^3	1000	50	293 F/g 16 F/cm^3	ref 33

[a]Density estimated from increase in mass versus initial sponge from ref 31.

heavy cell components. Unfortunately, most of the recently reported electrodes have thicknesses in the range of 1−10 μm, which is significantly thinner than the hundreds of micrometers to several millimeters thickness that practical applications require. The volumetric capacitance reported for these electrodes, a parameter that is crucial for devices requiring a compact energy storage device, is often quite high; however, this serves as a somewhat inflated figure, given that electrodes with low thickness require more inactive cell components, hurting the overall volumetric capacitance for the cell. Moreover, under significant mechanical strain such as bending, stretching, or compression, the electrodes cease to function due to electrode deformation and destruction, a problem that must be overcome for use in emerging applications such as wearable electronics. Compression is particularly challenging for foams of graphene and carbon nanotubes, which tend to bundle or restack when subjected to compressive strain.[23,24]

Mechanical stability of the electrodes under bending and stretching have been extensively researched given the prevalence of materials capable of withstanding such deformations, though research into EDLCs that retain their properties under compressive strain have been relatively sparse due to the rarity of porous and conductive three-dimensional structures that are capable of repeated compression without plastic deformation or fracture.[25−30] Several groups have demonstrated ultracompressible EDLCs that maintain capacitive performance up to ~50% compression. However, these EDLCs provided low gravimetric capacitances of less than 30 F/g and volumetric capacitance of ~0.1 F/cm^3, which necessitated the use of pseudocapacitive materials such as conducting polymers or metal oxides to increase the energy storage to ~300 F/g and 28 F/cm^3 albeit at a cost of degraded lifetime and reversibility of the electrodes.[31−34] The capacitance, rate performance, and other characteristics for compressible EDLCs and pseudocapacitors with graphene or nanotube based electrodes are presented in Table 1.

Herein, we demonstrate an EDLC with superelastic, fully carbon, 1.5 mm thick aerogels as electrodes that is capable of maintaining its capacitive performance at high rates of charge/discharge and high compressive strains. We have recently developed this type of material by coating the nodes of an isotropic single-wall carbon nanotube network within an aerogel with a few layers of graphene.[35] These graphene-coated nanotube aerogels fully recover their shapes after high values of compression, up to 90% strain, over many cycles without any plastic deformation or degradation in electrical conductivity.[35] When cycled in an EDLC configuration, the material showed high capacitance at high charge/discharge rates with aqueous and RTIL electrolytes in both uncompressed and compressed states with full recovery of shape and capacitance upon release. Further, the compressibility of the EDLC cells ultimately allowed us to achieve a volumetric capacitance that is 50−100 times higher than that of other reported compressible EDLCs.

MATERIALS AND METHODS

Fabrication of Graphene-Coated Nanotube Aerogels. CoMoCAT single-wall carbon nanotubes (CG200; SouthWest NanoTechnologies Inc.) with diameters of 1.01 ± 0.3 nm and lengths of 1 μm were used to fabricate nanotube aerogels. Methods for making various nanotube aerogels have been reported elsewhere.[35−37] Briefly, the nanotubes were mixed in sodium dodecylbenzenesulfonate (SDBS) solution in deionized water at a ratio of 1:10 by weight, forming a nanotube suspension with concentration of 1 mg/mL.[38] The suspension was sonicated for 2 h using a tip probe ultrasonicator and ultracentrifuged at 125 000g for 19 min to remove any bundles or impurities from the suspension. The supernatant was collected and analyzed using UV−vis−NIR spectroscopy (Varian Cary 5000) to determine the nanotube concentration, and then evaporated slowly until gel formation at 0.3 wt %.[39] The gel was liquefied and transferred into a mold of the desired shapes and sizes. After reformation of the gel, they were rinsed many times with water over the course of several hours and once with 1 M HNO_3 for 1 h to remove the surfactant, followed by thorough washing with deionized water. Energy-dispersive X-ray spectroscopy measurements on similarly produced gels showed that our fabrication process removed all surfactants and metal impurities from nanotubes.[35] The gels were transferred to a stainless steel hydrothermal reaction chamber (10 mL total volume) with 6 mL of 0.1 M D-glucose and 50 μL of hydrazine (50%, Acros Organics) in water and sealed. The chamber was heated to 60 °C for 30 min to aid infiltration of the glucose solution into the nanotube gel and then transferred to an oven at 185 °C for the cyclization and reduction of glucose into reduced graphene oxide.[40] After 6 h, the chamber was removed from the oven and cooled to room temperature. The gels were washed many times with water to remove any loose material, followed by a solution exchange with increasing concentrations of ethanol until the gels were in an anhydrous ethanol solution. At this point, the gels were dried with a critical point dryer (Tousimis Autosamdri-815, Series A) and subsequently pyrolyzed under nitrogen at 900 °C for 6 h to convert reduced graphene oxide to graphene.

Surface Area, Pore Diameter, and Microstructure Characterization. Specific surface area (SSA), pore diameter ($2r$), pore volume (V), and the pore diameter distribution (dV/dr) were measured through nitrogen adsorption and desorption at 77 K using a surface area analyzer (Micromeritics Gemini VII 2390) and the Brunauer−Emmet−Teller (BET) theory.[41] The pore diameter, pore volume, and pore diameter distribution were calculated using the density functional theory (DFT) and Barrett−Joyner−Halenda (BJH) methods from the desorption branch of the isotherms. The microstructure of the aerogels was imaged using an FEI Quanta 600 scanning electron microscopy (SEM). Transmission electron microscopy (TEM) micrographs were taken using a spherical aberration corrected FEI Titan 83.

Raman Spectroscopy. Raman Spectra of the samples were taken using a Raman spectrometer coupled to an inverted confocal

DOI: 10.1021/acsami.5b01384
ACS Appl. Mater. Interfaces 2015, 7, 5612−5618

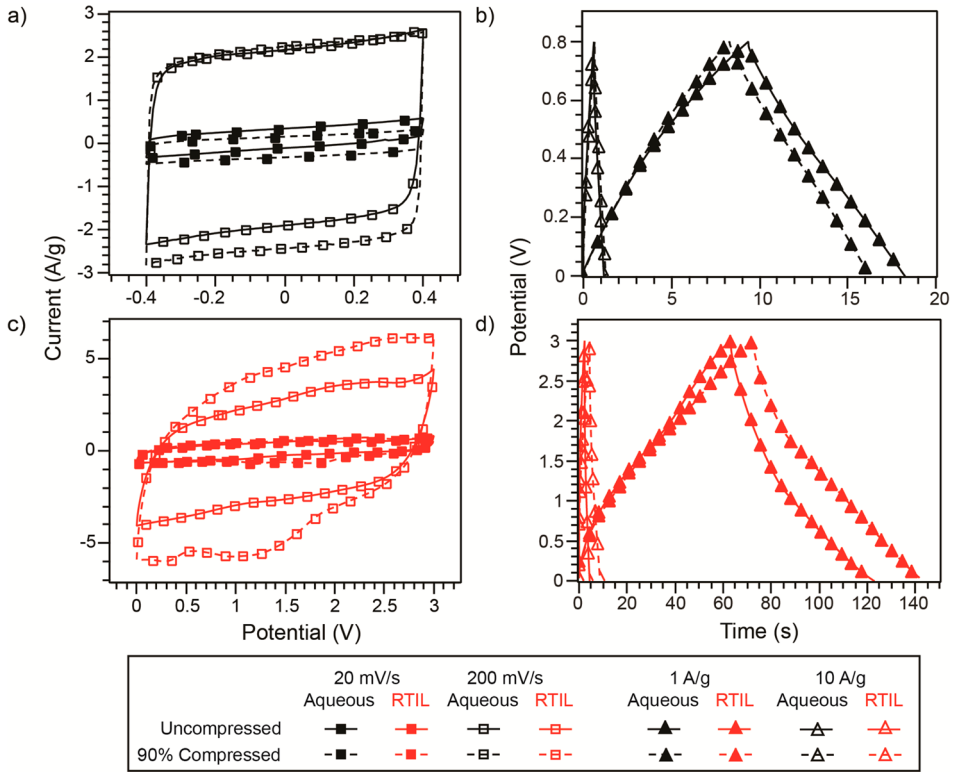

Figure 1. Electrochemical characteristics of graphene-coated nanotube aerogels in aqueous and room temperature ionic liquid (RTIL) electrolytes. (a and c) Cyclic voltammograms and (b and d) galvanostatic charge/discharge of cells with compressed and uncompressed electrodes in aqueous and RTIL electrolytes, respectively, at low (20 mV/s) and high (200 mV/s) scan rates.

microscope (inVia Raman microscope, Renishaw) with a 50× (0.4 NA) objective (Leica Microsystems) and a laser of wavelength 785 nm (1.58 eV). Laser power was set to 10 mW with a spot size of between 1 and 2 μm. Scans were taken with 30 s of exposure, and each spectrum is the result of three averages. All data was collected and analyzed using WiRE software (Renishaw). Spectra were normalized by the intensity of the G-band at 1580 cm^{-1}.

Electrochemical Characterization. Electrochemical cells were prepared using a parallel plate "button-cell" configuration (Figure S4, Supporting Information). Aerogels were attached to the center of a stainless steel disk using a small amount of conductive silver paste (DuPont 4929N) and left to dry in the oven for at least 1 h. After drying, the aerogels were infiltrated by an electrolyte under mild vacuum, either a 1 M aqueous solution of Na_2SO_4 or a small volume of the RTIL 1-ethyl-3-methylimidazolium bis(trifluoromethylsulfonyl)-imide (EMI-TFSI, Boulder Ionics). A porous polyolefin separator (Celgard, Inc.) was also infiltrated with electrolyte and then placed between both electrodes. We assembled the cell by placing shims between both disks and sealing the cell with PTFE tape. After assembly, the cell was attached to a potentiostat (Biologic SP-300), and all tests were performed using EC-Lab software.

RESULTS AND DISCUSSION

Material Characterization. We coated nanotube aerogels with graphene by a similar method that we previously reported, using glucose as the carbon source for graphene formation in this work instead of polyacrylonitrile polymer.[35] This graphene coating procedure preserved the morphology of the initial network, allowing for fabrication of various shapes and sizes of graphene-coated nanotube aerogels (Figure S1a, Supporting Information). We confirmed through SEM and TEM that the morphology of the network is similar to that which we have previously reported, with one or more layers of graphene coating of nearly all the nodes and ∼12% of the struts of the highly porous nanotube network (Figure S1b,c, Supporting Information).[35] Consequently, the density increased from 7 mg/mL for pristine nanotube aerogel to between 9 and 14 mg/mL after coating, yielding a total volume fraction of ∼0.7% and a porosity of >99%. The electrical conductivity slightly dropped from 1 S/cm for a nanotube aerogel to ∼0.8 S/cm after graphene coating. However, Raman spectroscopy (Figure S2, Supporting Information) confirmed that the graphene coating did not damage the nanotubes, and thus, we attribute the small decrease in conductivity to the accumulation of disordered graphene layers at the nodes.[35,37] Nitrogen adsorption measurements (Figure S3a, Supporting Information), in conjunction with the BET method, gave an SSA for the graphene of 698 m^2/g, which is somewhat lower than a pristine nanotube aerogel (1291 m^2/g) due to the graphene coating the surface and nodes but still significantly higher than many other nanotube foams.[37,41] The pores of the aerogel were primarily between 2 and 30 nm in diameter, and most were below 10 nm, as determined by BJH and DFT analyses on the desorption isotherms (Figure S3b, Supporting Information), which should allow for facile ionic transport.[42,43]

Electrochemical Performance. The properties of the graphene-coated nanotube aerogels, namely, their high surface area, electrical conductivity, and porosity, make them excellent candidates for EDLC electrodes. We investigated the electrochemical properties of these aerogels in both uncompressed and compressed states using home-built electrochemical cells that had a two-electrode coin cell configuration (Figure S4, Supporting Information) and with two different electrolytes: an aqueous electrolyte of 1 M Na_2SO_4 and an RTIL (1-ethyl-3-methylimidazolium bis(trifluoromethylsulfonyl)imide). The thickness of the uncompressed electrode for all our experiments

DOI: 10.1021/acsami.5b01384
ACS Appl. Mater. Interfaces 2015, 7, 5612−5618

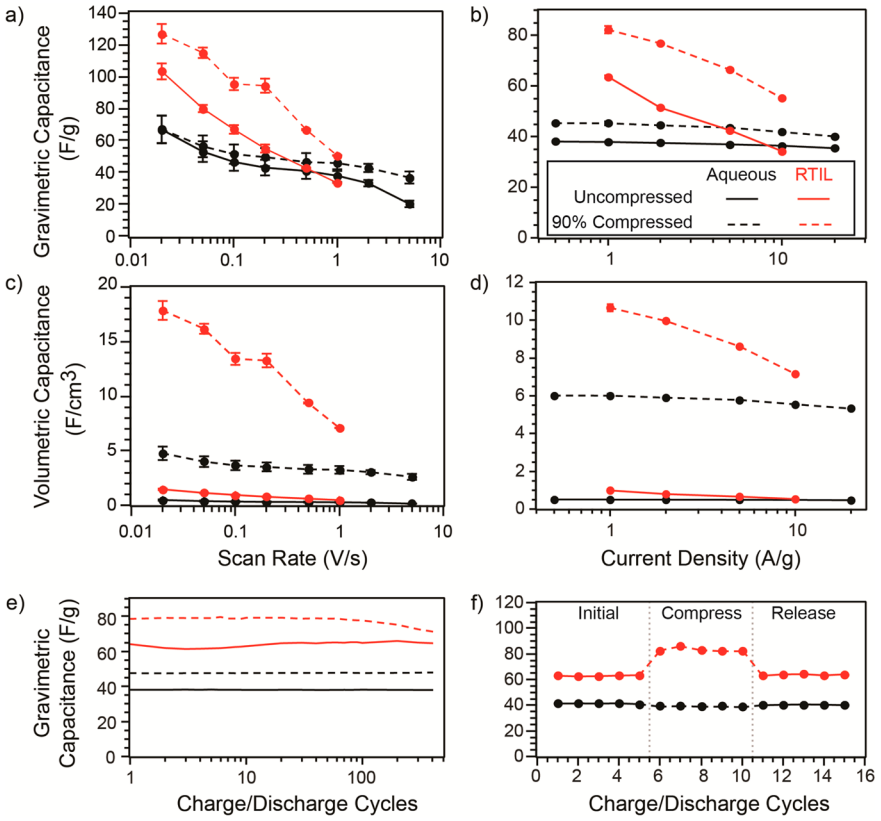

Figure 2. Capacitance characteristics. Legends are shown in panel (b). Gravimetric capacitance of the cells under (a) cyclic and (b) galvanostatic conditions with aqueous and RTIL electrolytes. Volumetric capacitance of the cells under (c) cyclic and (d) galvanostatic conditions with aqueous and RTIL electrolytes. (e) Cycling stability of the electrodes with aqueous and RTIL electrolytes in uncompressed and compressed states at a current density of 1 A/g. (f) Compression and recovery of the capacitance for electrodes in aqueous and RTIL electrolytes, taken at a current density of 1 A/g.

was 1.5 mm and is significantly thicker than most other reported electrode thicknesses. We varied the compression of the cells by varying the number of shims during construction (Figure S4, Supporting Information). Cyclic voltammetry (CV) measurements with aqueous electrolyte showed a near-ideal rectangular shape over a broad range of scan rates, from 20 mV/s to 2 V/s, in both uncompressed and compressed states, indicative of highly capacitive behavior and low resistance of the cells. We show two representative CV curves at 20 and 200 mV/s in Figure 1a. The near-ideal rectangular shape of the CV curves, even at high scan rates and at 90% compression, suggest that the ionic and electronic transport for this system was unaffected by compressive strain. For the cell with RTIL electrolyte, CV (Figure 1c) measurements also showed a rectangular shape with several broad faradaic peaks throughout the potential range. Because the aerogel fabrication process removed any metallic catalyst impurities from the nanotube dispersion, as verified previously by energy-dispersive X-ray spectroscopy,[35] we postulate that the faradaic response likely arose due to reactions between RTIL and functional groups present on graphene; similar faradaic peaks have been reported for EDLC electrodes of similarly produced graphene.[44] These peaks significantly diminished as the scan rate increased, likely due to the relatively slow kinetics of the faradaic reactions. Cells with both aqueous and RTIL electrolytes showed a slight increase in the capacitance under compression, which we attribute to fuller utilization of the active surface area due to decreased ionic transport lengths. The galvanostatic charge/discharge (GCD) behavior for the cells using the aqueous electrolyte (Figure 1b) showed straight and symmetric curves from 1 to 20 A/g as a result of their highly capacitive character. This behavior was retained under 90% compression, confirming that the material's electrochemical response was largely invariant to compressive strain. Current characteristics for the cells using the RTIL electrolyte (Figure 1d) showed similar linear and symmetric behavior, though with a more significant vertical drop at high current densities caused by the internal resistance (IR) losses within the cell. Compression of the cell decreased the IR drop, which suggests an improvement in ionic transport.

The current responses from measurements of CV versus scan rates and GCD versus current densities enabled us to ascertain the rate capability of the electrodes. The gravimetric capacitance of the cells using aqueous and RTIL electrolytes for CV and GCD tests are shown in Figures 2a,b. Cells with uncompressed and compressed electrodes both showed comparable initial gravimetric capacitances of ~70 F/g. As the scan rate and current density were increased, both showed nearly identical performance up to very high scan rates of 5 V/s and 20 A/g, illustrating the strain-invariance of the transport through the electrodes. We note that cells with thick electrodes typically display significantly diminished capacitive performance under high-rate operations. However, due to the facile ion transport through our electrodes, gravimetric capacitance showed negligible drop, even with 1.5 mm thick electrodes and at high scan rates. In addition, the gravimetric capacitance of a cell with 1.5 mm thick electrodes was comparable to that of a cell with electrodes nearly an order of magnitude thinner at

DOI: 10.1021/acsami.5b01384
ACS Appl. Mater. Interfaces 2015, 7, 5612−5618

low scan rates, further confirming the unobstructed transport of ions through these electrodes (Figure S5, Supporting Information). For the cells using an RTIL electrolyte, we found that for all scan rates and current densities, the cells with compressed electrodes showed a higher gravimetric capacitance than the cells with uncompressed electrodes, likely due to the incomplete utilization of the surface area because of the low conductivity of the ionic liquid. However, both displayed nearly identical capacitance loss as the charge/discharge rate was increased, again showing the strain invariance of the ionic transport through the electrodes. The strain invariance of ion transport through the electrodes also resulted in the current response of the cell with 1.5 mm electrodes after compressing to 150 μm thick to be nearly identical to that of a cell with electrodes of similar thickness.

We exploited the strain-invariant capacitive behavior of our electrodes to construct cells with high values of volumetric capacitance. Figure 2c,d show that for both electrolyte systems, a 90% compression resulted in over an order of magnitude enhancement in the volumetric capacitance with the cells using an aqueous electrolyte showing almost 5 F/cm^3 and the cells using an RTIL showing 18 F/cm^3. To compare, compressible EDLCs with multiwalled carbon nanotube sponge electrodes had a volumetric capacitance of ~0.1 F/cm^3.[31] Further, the volumetric capacitance of our EDLCs with RTIL electrolyte approached volumetric capacitance values for compressible pseudocapacitors, which have been reported to be between ~15 and 30 F/cm^3.[32−34]

To determine the stability of the capacitance over many charge/discharge cycles, we cycled the cell galvanostatically several hundred times for each cell at 1 A/g. Figure 2e shows that for the aqueous cells, there is less than 3% change between the initial capacitance and the capacitance after 400 charge/discharge cycles, indicative of the high structural stability of the electrodes. Similarly, the RTIL cells showed nearly identical capacitance after 400 charge/discharge cycles, with less than 10% loss in capacitance. The capacitance of the cells with either aqueous or RTIL electrolytes was also highly stable when the electrodes were compressed by 90% (Figure 2e). We also tested the stability of the electrochemical properties of these electrodes after mechanical compression by measuring the capacitance after compression and release of the cells. Both aqueous and RTIL cells showed full recovery of the initial capacitance after multiple compression and release cycles at 90% compressive strain (Figure 2f), confirming that this compression did not cause any destruction to the aerogel or structural changes that would decrease capacitance. We tabulated the capacitance, rate performance, and other characteristics for our compressible EDLCs to those of other compressible EDLCs and pseudocapacitors with graphene or nanotube based electrodes in Table 1.

We further quantified the electrical and ionic transport of cells with aqueous and RTIL electrolytes in uncompressed and compressed states at low and high charge/discharge rates by analyzing the frequency response using electrochemical impedance spectroscopy (EIS). Figure 3a shows the Nyquist plots of cells with electrodes in uncompressed and compressed states. The response for all cells was characteristic of an EDLC, with a semicircle near the x axis corresponding to high-frequency response and a linear region corresponding to low-frequency response. At high frequencies, all cells displayed x axis intercepts below 5 Ω, indicative of low series resistance.[45,46] Both cells with aqueous and RTIL electrolytes showed a

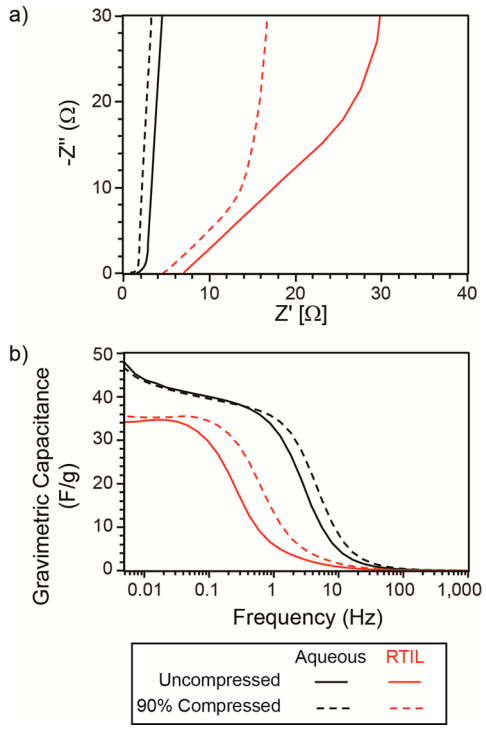

Figure 3. Frequency response of graphene-coated nanotube aerogels in aqueous and RTIL electrolytes. (a) Nyquist plot of EDLCs with both uncompressed and compressed electrodes for frequencies between 500 kHz and 5 mHz. (b) Bode plot of EDLCs with both uncompressed and compressed electrodes. The capacitance for the cells was determined by approximating the response of the cell as a frequency-dependent resistor and capacitor in series.

decrease in series resistance because of compression, given the diminished resistance to ionic transport from a shorter path length. The compressed cells also displayed a less pronounced Warburg resistance, shown by the decreased 45° transition between the high- and low-frequency regions of the EIS spectra.[47] The Warburg resistance was significantly more pronounced for cells using RTIL electrolytes because of the electrolyte's lower electrical conductivity and higher viscosity. The Bode plot in Figure 3b shows the real portion of the capacitance for each of the cells as a function of the frequency (f). The lack of faradaic reactions at the potential used for the EIS tests resulted in the cells using an RTIL electrolyte displaying lower real capacitance than what was observed for CV and GCD tests. For both cells, compressions of the electrodes shifted the curves to higher frequencies, indicative of higher capacitance retention at increased charge/discharge rates, and were consistent with the results from CV and GCD testing.

CONCLUSIONS

We have developed an EDLC that is capable of high rate performance, even at 90% mechanical compression with aqueous and RTIL electrolytes by utilizing thick (1.5 mm), superelastic graphene-coated nanotube aerogels as electrodes. These electrodes displayed nearly ideal supercapacitive properties because of their high surface area, porosity, and electrical conductivity. The electrochemical performance of these aerogels was largely invariant to compressive strains up to 90%, with no increase in resistance or decrease in capacitance. Moreover, we exploited this controllable compressibility and

DOI: 10.1021/acsami.5b01384
ACS Appl. Mater. Interfaces 2015, 7, 5612−5618

recoverability to achieve volumetric capacitance of 5 and 18 F/cm^3 with aqueous and RTIL electrolyte, respectively, without causing increased diffusive resistance, allowing for simultaneous ultracompressibility and high-rate charge/discharge cycling, in addition to volumetric capacitance 50−100 times greater than that of a comparable compressible EDLC. Because the cell does not rely on pseudocapacitive functionalities for mechanical stability and/or capacitive performance, the cell displayed excellent capacitance retention on repeated cycling and is anticipated to continue this trend for many more cycles. This material serves as an excellent platform for exploring the possibility of electrode structures that are capable of undergoing large compressive deformations without degradation for use in applications such as electric vehicles and wearable electronics.

■ ASSOCIATED CONTENT

Supporting Information

Structural characterization of the graphene-coated nanotube aerogels, Raman spectra of the pristine and graphene-coated nanotube aerogels, schematic representation of the compression test cells, and electrode thickness dependent capacitance for cells with aqueous electrolyte. This material is available free of charge via the Internet at http://pubs.acs.org.

■ AUTHOR INFORMATION

Corresponding Author

*Tel.: +1 412 268 8999. Fax: +1 412 268 7596. E-mail: mohammad@cmu.edu.

Author Contributions

M.F.I. developed and designed the project. E.W. carried out experiments and collected and analyzed data. M.F.I. gave technical and conceptual advice. E.W. and M.F.I. wrote the manuscript.

Notes

The authors declare no competing financial interest.

■ ACKNOWLEDGMENTS

The authors thank T. Nuhfer for his assistance with TEM. This work was supported by the National Science Foundation through grants CMMI-1335417 and the NSF NEEP (Nanotechnology, Environmental Effects, and Policy) IGERT fellowship program (0966227).

■ REFERENCES

(1) Wang, G.; Zhang, L.; Zhang, J. A Review of Electrode Materials for Electrochemical Supercapacitors. *Chem. Soc. Rev.* **2012**, *41* (2), 797−828.

(2) Zhang, L. L.; Zhao, X. S. Carbon-based Materials as Supercapacitor Electrodes. *Chem. Soc. Rev.* **2009**, *38* (9), 2520−2531.

(3) Du Pasquier, A.; Plitz, I.; Menocal, S.; Amatucci, G. A Comparative Study of Li-ion Battery, Supercapacitor and Nonaqueous Asymmetric Hybrid Devices for Automotive Applications. *J. Power Sources* **2003**, *115* (1), 171−178.

(4) Zhai, Y.; Dou, Y.; Zhao, D.; Fulvio, P. F.; Mayes, R. T.; Dai, S. Carbon Materials for Chemical Capacitive Energy Storage. *Adv. Mater.* **2011**, *23* (42), 4828−4850.

(5) Simon, P.; Gogotsi, Y. Materials for Electrochemical Capacitors. *Nat. Mater.* **2008**, *7* (11), 845−854.

(6) Liu, C.; Li, F.; Ma, L.-P.; Cheng, H.-M. Advanced Materials for Energy Storage. *Adv. Mater.* **2010**, *22* (8), E28−E62.

(7) Paek, E.; Pak, A. J.; Hwang, G. S. Curvature Effects on the Interfacial Capacitance of Carbon Nanotubes in an Ionic Liquid. *J. Phys. Chem. C* **2013**, *117* (45), 23539−23546.

(8) Endo, M.; Maeda, T.; Takeda, T.; Kim, Y. J.; Koshiba, K.; Hara, H.; Dresselhaus, M. S. Capacitance and Pore-Size Distribution in Aqueous and Nonaqueous Electrolytes Using Various Activated Carbon Electrodes. *J. Electrochem. Soc.* **2001**, *148* (8), A910−A914.

(9) Qu, D.; Shi, H. Studies of Activated Carbons Used in Double-Layer Capacitors. *J. Power Sources* **1998**, *74* (1), 99−107.

(10) Gamby, J.; Taberna, P. L.; Simon, P.; Fauvarque, J. F.; Chesneau, M. Studies and Characterizations of Various Activated Carbons Used for Carbon/Carbon Supercapacitors. *J. Power Sources* **2001**, *101* (1), 109−116.

(11) Bin, X.; Yue, S.; Sui, Z.; Zhang, X.; Hou, S.; Cao, G.; Yang, Y. What is the Choice for Supercapacitors: Graphene or Graphene Oxide? *Energy Environ. Sci.* **2011**, *4* (8), 2826−2830.

(12) Izadi Najafabadi, A.; Yasuda, S.; Kobashi, K.; Yamada, T.; Futaba, D. N.; Hatori, H.; Yumura, M.; Iijima, S.; Hata, K. Extracting the Full Potential of Single-Walled Carbon Nanotubes as Durable Supercapacitor Electrodes Operable at 4 V with High Power and Energy Density. *Adv. Mater.* **2010**, *22* (35), E235−E241.

(13) Jiang, H.; Lee, P. S.; Li, C. 3D Carbon-based Nanostructures for Advanced Supercapacitors. *Energy Environ. Sci.* **2012**, *6* (1), 41−53.

(14) Kaempgen, M.; Chan, C. K.; Ma, J.; Cui, Y.; Gruner, G. Printable Thin Film Supercapacitors Using Single-Walled Carbon Nanotubes. *Nano Lett.* **2009**, *9* (5), 1872−1876.

(15) Liu, C.; Yu, Z.; Neff, D.; Zhamu, A.; Jang, B. Z. Graphene-based Supercapacitor with an Ultrahigh Energy Density. *Nano Lett.* **2010**, *10* (12), 4863−4868.

(16) Pan, H.; Li, J.; Feng, Y. P. Carbon Nanotubes for Supercapacitor. *Nanoscale Res. Lett.* **2010**, *5* (3), 654−668.

(17) Zhang, H.; Cao, G.; Yang, Y. Carbon Nanotube Arrays and Their Composites for Electrochemical Capacitors and Lithium-ion Batteries. *Energy Environ. Sci.* **2009**, *2* (9), 932−943.

(18) Zhang, J.; Jiang, D.; Peng, H.-X.; Qin, F. Enhanced Mechanical and Electrical Properties of Carbon Nanotube Buckypaper by in Situ Cross-Linking. *Carbon* **2013**, *63*, 125−132.

(19) Zhang, L. L.; Zhou, R.; Zhao, X. S. Graphene-based Materials as Supercapacitor Electrodes. *Journal of Materials Chemistry A* **2010**, *20* (29), 5983−5992.

(20) Cheng, Q.; Tang, J.; Ma, J.; Zhang, H.; Shinya, N.; Qin, L.-C. Graphene and Carbon Nanotube Composite Electrodes for Supercapacitors with Ultra-High Energy Density. *Phys. Chem. Chem. Phys.* **2011**, *13* (39), 17615−17624.

(21) El-Kady, M. F.; Strong, V.; Dubin, S.; Kaner, R. B. Laser Scribing of High-Performance and Flexible Graphene-based Electrochemical Capacitors. *Science* **2012**, *335* (6074), 1326−1330.

(22) Zhou, C.; Liu, J. Carbon Nanotube Network Film Directly Grown on Carbon Cloth for High-Performance Solid-State Flexible Supercapacitors. *Nanotechnology* **2013**, *25* (3), 035402.

(23) Gui, X.; Zeng, Z.; Zhu, Y.; Li, H.; Lin, Z.; Gan, Q.; Xiang, R.; Cao, A.; Tang, Z. Three-Dimensional Carbon Nanotube Sponge-Array Architectures with High Energy Dissipation. *Adv. Mater.* **2014**, *26* (8), 1248−1253.

(24) He, Y.; Chen, W.; Li, X.; Zhang, Z.; Fu, J.; Zhao, C.; Xie, E. Freestanding Three-Dimensional Graphene/MnO_2 Composite Networks As Ultralight and Flexible Supercapacitor Electrodes. *ACS Nano* **2013**, *7* (1), 174−182.

(25) Choi, B. G.; Yang, M.; Hong, W. H.; Choi, J. W.; Huh, Y. S. Flexible Solid-State Supercapacitors based on Carbon Nanoparticles/MnO_2 Nanorods Hybrid Structure. *ACS Nano* **2012**, *6* (1), 656−661.

(26) Gwon, H.; Kim, H.-S.; Lee, K. U.; Seo, D.-H.; Park, Y. C.; Lee, Y.-S.; Ahn, B. T.; Kang, K. Flexible Energy Storage Devices based on Graphene Paper. *Energy Environ. Sci.* **2011**, *4* (4), 1277−1283.

(27) Hu, S.; Rajamani, R.; Yu, X. Flexible Solid-State Paper based Carbon Nanotube Supercapacitor. *Appl. Phys. Lett.* **2012**, *100* (10), 104103.

(28) Meng, C.; Liu, C.; Chen, L.; Hu, C.; Fan, S. Highly Flexible and All-Solid-State Paperlike Polymer Supercapacitors. *Nano Lett.* **2010**, *10* (10), 4025−4031.

(29) Pushparaj, V. L.; Shaijumon, M. M.; Kumar, A.; Murugesan, S.; Ci, L.; Vajtai, R.; Linhardt, R. J.; Nalamasu, O.; Ajayan, P. M. Flexible

DOI: 10.1021/acsami.5b01384
ACS Appl. Mater. Interfaces 2015, 7, 5612−5618

Energy Storage Devices based on Nanocomposite Paper. *Proc. Natl. Acad. Sci. U.S.A.* **2007**, *104* (34), 13574−13577.
(30) Tao, J.; Liu, N.; Ma, W.; Ding, L.; Li, L.; Su, J.; Gao, Y. Solid-State High Performance Flexible Supercapacitors based on Polypyrrole-MnO_2-Carbon Fiber Hybrid Structure. *Sci. Rep.* **2013**, *3*, 1−7.
(31) Li, P.; Kong, C.; Shang, Y.; Shi, E.; Yu, Y.; Qian, W.; Wei, F.; Wei, J.; Wang, K.; Zhu, H.; Cao, A.; Wu, D. Highly Deformation-Tolerant Carbon Nanotube Sponges as Supercapacitor Electrodes. *Nanoscale* **2013**, *5* (18), 8472−8479.
(32) Li, P.; Shi, E.; Yang, Y.; Shang, Y.; Peng, Q.; Wu, S.; Wei, J.; Wang, K.; Zhu, H.; Yuan, Q.; Cao, A.; Wu, D. Carbon Nanotube−Polypyrrole Core−Shell Sponge and its Application as Highly Compressible Supercapacitor Electrode. *Nano Res.* **2013**, *7* (2), 209−218.
(33) Li, P.; Yang, Y.; Shi, E.; Shen, Q.; Shang, Y.; Wu, S.; Wei, J.; Wang, K.; Zhu, H.; Yuan, Q.; Cao, A.; Wu, D. Core-Double-Shell, Carbon Nanotube@Polypyrrole@MnO_2 Sponge as Freestanding, Compressible Supercapacitor Electrode. *ACS Appl. Mater. Interfaces* **2014**, *6* (7), 5228−5234.
(34) Zhao, Y.; Liu, J.; Hu, Y.; Cheng, H.; Hu, C.; Jiang, C.; Jiang, L.; Cao, A.; Qu, L. Highly Compression-Tolerant Supercapacitor based on Polypyrrole-Mediated Graphene Foam Electrodes. *Adv. Mater.* **2012**, *25* (4), 591−595.
(35) Kim, K. H.; Oh, Y.; Islam, M. F. Graphene Coating Makes Carbon Nanotube Aerogels Superelastic and Resistant to Fatigue. *Nat. Nanotechnol.* **2012**, *7* (9), 562−566.
(36) Bryning, M. B.; Milkie, D. E.; Islam, M. F.; Hough, L. A.; Kikkawa, J. M.; Yodh, A. G. Carbon Nanotube Aerogels. *Adv. Mater.* **2007**, *19* (5), 661−664.
(37) Kim, K. H.; Oh, Y.; Islam, M. F. Mechanical and Thermal Management Characteristics of Ultrahigh Surface Area Single-Walled Carbon Nanotube Aerogels. *Adv. Funct. Mater.* **2012**, *23* (3), 377−383.
(38) Islam, M. F.; Rojas, E.; Bergey, D. M.; Johnson, A. T.; Yodh, A. G. High Weight Fraction Surfactant Solubilization of Single-Wall Carbon Nanotubes in Water. *Nano Lett.* **2003**, *3* (2), 269−273.
(39) Hough, L. A.; Islam, M. F.; Janmey, P. A.; Yodh, A. G. Viscoelasticity of Single Wall Carbon Nanotube Suspensions. *Phys. Rev. Lett.* **2004**, *93* (16), 168102.
(40) Tang, L.; Li, X.; Ji, R.; Teng, K. S.; Tai, G.; Ye, J.; Wei, C.; Lau, S. P. Bottom-Up Synthesis of Large-Scale Graphene Oxide Nanosheets. *J. Mater. Chem. A* **2012**, *22* (12), 5676−5683.
(41) Brunauer, S.; Emmett, P. H.; Teller, E. Adsorption of Gases in Multimolecular Layers. *J. Am. Chem. Soc.* **1938**, *60* (2), 309−319.
(42) Barrett, E. P.; Joyner, L. G.; Halenda, P. P. The Determination of Pore Volume and Area Distributions in Porous Substances. I. Computations from Nitrogen Isotherms. *J. Am. Chem. Soc.* **1951**, *73* (1), 373−380.
(43) Monson, P. A. Understanding Adsorption/Desorption Hysteresis for Fluids in Mesoporous Materials using Simple Molecular Models and Classical Density Functional Theory. *Microporous Mesoporous Mater.* **2012**, *160*, 47−66.
(44) Wei, L.; Sevilla, M.; Fuertes, A. B.; Mokaya, R.; Yushin, G. Polypyrrole-Derived Activated Carbons for High-Performance Electrical Double-Layer Capacitors with Ionic Liquid Electrolyte. *Adv. Funct. Mater.* **2011**, *22* (4), 827−834.
(45) Li, X.; Rong, J.; Wei, B. Electrochemical Behavior of Single-Walled Carbon Nanotube Supercapacitors under Compressive Stress. *ACS Nano* **2010**, *4* (10), 6039−6049.
(46) Taberna, P. L.; Simon, P.; Fauvarque, J. F. Electrochemical Characteristics and Impedance Spectroscopy Studies of Carbon-Carbon Supercapacitors. *J. Electrochem. Soc.* **2003**, *150* (3), A292−A300.
(47) Park, S.-M.; Yoo, J.-S. Electrochemical Impedance Spectroscopy for Better Electrochemical Measurements. *Anal. Chem.* **2003**, *75* (21), 455A−461A.

NOTE ADDED AFTER ASAP PUBLICATION

This paper published ASAP on March 2, 2015. The Acknowledgment section was corrected and the revised version was reposted on March 11, 2015.

DOI: 10.1021/acsami.5b01384
ACS Appl. Mater. Interfaces 2015, 7, 5612−5618